An Ion-Sensitive Floating Gate FET Model: Operating Principles and Electrofluidic Gating

Matti Kaisti, Qi Zhang, Alok Prabhu, Ari Lehmusvuori, Arifur Rahman, *Senior Member, IEEE*, and Kalle Levon

***Abstract*— We present a model that can be used to compute the charging and potential at any point of the electrochemical system comprising the ion-sensitive floating gate FET (ISFGFET) exposed to an electrolyte solution. In contrast to ion-sensitive FETs, the sensor has an additional control input gate. The model predicts the possibility for electrofluidic gating when the control gate (CG) is used in conjunction with a reference electrode (RE). Electrofluidic gating is the field-effect control over the electric double layer. We consider the applicability of electrofluidic gating in realizable devices and simulate the relationships between oxide properties and electrolyte solution to varying potentials of the CG and the RE. The oxide/electrolyte solution model is merged to the SPICE model of the transistor to create a unified model that can be used to simulate the transfer characteristics of the sensor in absolute terms to change input and electrolyte solution conditions. We simulate the sensor transfer characteristics with common Al_2O_3 surface to change the pH of the electrolyte solution and compare them to measurements. The results clarify the operation of ISFGFET and its applicability in electrofluidic gating.**

***Index Terms*— Biosensor, electrofluidic gating, floating gate, ion-sensitive FET (ISFET), ion-sensitive floating gate FET (ISFGFET).**

I. Introduction

TRANSISTOR-BASED biosensors have great promise as biological and/or chemical sensors. These sensors have the possibility for robust, small size, cost-effective, and portable label-free detection without the need for bulky optics or fluorescent dyes. The concept of ion-sensitive FET (ISFET) was described in the 1970s by Bergveld [1] and ISFET was first used as a pH meter and recently to sequence the human genome [2]. The first ISFETs were MOSFETs with a removed gate metal where the underlying oxide was exposed to a saline solution. The first ISFET exploiting the FG structure with a control gate (CG) was proposed in [3]. Similar structures have since been described by our group [4], [5] and by several others [6]–[8]. The gate of the ISFET is replaced by a floating node that is capacitively coupled to two inputs: 1) a sensing gate (SG) and 2) a CG, both of which can be used to modulate the current flow through the transistor. A recent study by Jayant *et al.* [8] is closely related to this paper. A similar sensor concept and a surface programming is elucidated by considering the electric field of the sensing oxide.

We extend this by presenting a unified model that is able to relate any system parameter to the sensor output with the ability to extract the sensor transfer characteristics and changes in them with varying sensing and operating conditions. We apply a new interface model developed in [9] to our ion-sensitive FG FET (ISFGFET) concept. The model relies on the site binding theory and double-layer description of the electrolyte solution similarly as the generally accepted model in [10], but with clear improvements. We do not uncouple the electronic part, and the electrolyte solution has been done in ISFET models [10], [11].

In our ISFGFET concept, the interplay with the reference electrode (RE) and the CG can be used for the electrofluidic gating, i.e., control the charging of the surface and the ionic screening layer via the field effect. Electrofluidic gating has been demonstrated to have new intriguing possibilities in fluidic devices, such as electro-osmotic flow, control the transport of charged proteins, and charge regulation of nanopores [9], [12]–[15] and we envision the possibilities of enhanced hybridization [16], [17] in DNA sensors that rely on probe immobilization on the sensing surface and direct measurement of the intrinsic charge of DNA molecules.

We concentrate on the device characteristics and on the interplay between the CG and the RE. In a similar FG structure, a quantitative probing of the surface charge without a RE has been shown [18]. However, this does not allow direct control over the charging of the surface and the ionic screening layer, since the potential over the sensing membrane and electrolyte solution cannot be controlled.

We validate the proposed model via experiments with the ISFGFET where the Si_3N_4 at the SG is cut to expose aluminum pad to which a native pH sensitive aluminum oxide forms. This approach removes significant threshold voltage variations resulting from the passivation layer trapped charge [19] and has only modestly reduced sensor tranconductance compared with the nMOS at the heart of the device.

This paper is organized as follows In Section II, we describe the FG transistor and proceed to the electrochemical model in Section III. In Section IV, we discuss the

Manuscript received January 14, 2015; revised May 25, 2015; accepted May 28, 2015. The work of M. Kaisti was supported by the Jenny and Antti Wihuri Foundation. The review of this paper was arranged by Editor I. Kymissis.

M. Kaisti is with the Technology Research Center, University of Turku, Turku 20014, Finland (e-mail: mkaist@utu.fi).

Q. Zhang, A. Prabhu, and K. Levon are with the Department of Chemical and Biomolecular Engineering, New York University, Brooklyn, NY 11201 USA (e-mail: qz260@nyu.edu; alokprabhu@yahoo.com; kalle.levon@gmail.com).

A. Lehmusvuori is with the Department of Biochemistry, University of Turku, Turku 20520, Finland (e-mail: artule@utu.fi).

A. Rahman is with Altera Corporation, San Jose, CA 95134 USA (e-mail: arifoni@yahoo.com).

Color versions of one or more of the figures in this paper are available online at http://ieeexplore.ieee.org.

Digital Object Identifier 10.1109/TED.2015.2441878

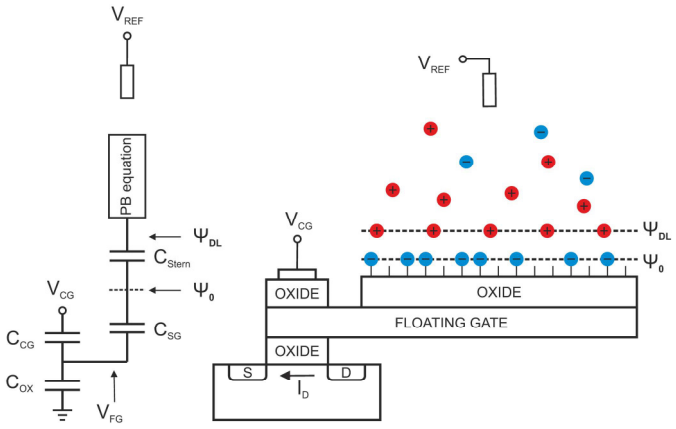

Fig. 1. Simplified diagram of the ISFGFET (right) and its equivalent circuit (left). The solution is modeled as a condensed Stern layer with its equivalent capacitance C_{Stern} and by the diffuse layer described by the Poisson–Boltzmann equation. The FGFET structure is modeled as a single-gate nMOS with an added FG and a CG capacitor C_{CG} and an SG capacitor C_{SG}. These capacitors couple V_{CG} and Ψ_0 to the FG. The channel oxide capacitance is C_{OX}.

device operation through the simulation results, including the ISFGFET sensitivity, surface programming, including electrofluidic gating, and finally the sensor operation modes. Before concluding this paper in Section VI, we present the experimental verification of the model in Section V.

II. Floating Gate Transistor

The ISFGFET is an n-channel MOSFET with two input gates that are capacitively coupled to a common FG. Simplified diagram of the ISFGFET is shown in Fig. 1. More detailed device description is given in [20]. It performs a weighted sum of the inputs voltages, and this sum is seen at the FG. ISFGFET operates with capacitively coupled voltage nodes and the net charge Q at the FG is fixed and can be expressed as [21]

$$Q = \sum_i (V_{\text{FG}} - V_i) C_i \tag{1}$$

where V_{FG} is the potential at the FG, and V_i and C_i are the ith input gate potential and capacitance, respectively. In our analysis, we assume that the transistor bulk is grounded.

The sensing area in the design layout is located above and aside from the active parts of the sensor [20]. Therefore, we omit the parasitic capacitances from the SG to the source, the drain and bulk in our analysis, since they provide no further insights in our analysis. However, these can be easily included into the model, if required. A detailed analysis of the ISFET with parasitic capacitances has been presented earlier [19]. The simplified V_{FG} is given as

$$V_{\text{FG}} = \frac{V_{\text{CG}} C_{\text{CG}} + \Psi_0 C_{\text{SG}}}{C_{\text{TOT}}} + \frac{Q}{C_{\text{TOT}}} \tag{2}$$

where $C_{\text{TOT}} = C_{\text{CG}} + C_{\text{SG}} + C_{\text{OX}}$. C_{CG} and C_{SG} are the CG capacitance and SG capacitance, respectively, and C_{OX} is the gate oxide capacitance, and Ψ_0 and V_{CG} are the sensing surface and CG potentials, respectively.

The SG capacitance in ISFETs is not well understood. It is not the conventional capacitor with two parallel plates around a dielectric medium, but rather it is a stacked structure of metal/oxide/solution [22]. Several capacitance correcting schemes have been proposed for ISFETs manufactured in unmodified CMOS processes [19], [22]. In these designs, it is common that the sensing membrane extends over the entire chip, and it is not constrained only to lie on the SG area.

In contrast, an FG design, where a sensing area was exposed through postprocessing steps, the sensing oxide capacitance was found to follow the physical sensing area accurately [23]. Our device resembles most the latter case, and therefore, we do not apply any correcting factors to C_{SG}.

It is V_{FG} along with the transistor physical properties that set the current through the transistor. In common equations describing MOSFET operation, V_{GS} is replaced with potential difference between the FG and the source. In this paper, this potential equals V_{FG}, since source node is grounded. V_{FG} and drain current relationship is simulated with the foundry specific SPICE model.

III. Model of the Electrochemical System

The early models of oxide surface sensitivity to bulk solution pH (pH_B) considered the Nernst equation. It predicted that a unit change in a pH_B creates a potential shift at the oxide surface as 2.3 kT/e [V/pH_B], where $kT/e \approx 25$ mV is the thermal voltage. This relation described by the Nernst equation is reasonable for glass electrodes but not for insulator interfaces that are neither electric nor ionic conductors. Modern theories rely on models originating from colloid chemistry where the site-dissociation model is combined with the double-layer theory [10], [24], [25]. We consider a general interface model described in [9]. The potentials V_{FG}, Ψ_0, Ψ_{DL}, and the RE potential V_{REF} shown in Fig. 1 can be related by

$$\sigma_{\text{SG}} = C_{\text{SG}}(V_{\text{FG}} - \Psi_0) \tag{3}$$

$$\sigma_{\text{DL}} = C_{\text{Stern}}(\Psi_0 - \Psi_{\text{DL}}). \tag{4}$$

A constant Stern layer capacitance $C_{\text{Stern}} = 18\ \mu\text{F/cm}^2$ is obtained assuming a 5 Å charge separation with dielectric constant of 10. The surface charge σ_0 consists of the double-layer charge σ_{DL} and the SG charge σ_{SG}, and thus

$$\sigma_0 = \sigma_{\text{DL}} - \sigma_{\text{SG}}. \tag{5}$$

The reactions at the oxide surface with amphoteric surface groups can be explained according to the following dissociation reactions [26]:

$$S \cdot \text{OH} \overset{K_A}{\rightleftharpoons} S \cdot O^- + H_B^+(\text{aq}) \tag{6}$$

$$S \cdot \text{OH}_2^+ \overset{K_B}{\rightleftharpoons} S \cdot \text{OH} + H_B^+(\text{aq}) \tag{7}$$

where S describes the surface with a bonded hydroxyl group. The sensing surface charge is then given by

$$\sigma_0 = -e\Gamma^{O-} + e\Gamma^{\text{OH}_2^+} \tag{8}$$

where the total fixed number of binding sites per unit area is $N_s = \Gamma = \Gamma^{O-} + \Gamma^{\text{OH}_2^+} + \Gamma^{\text{OH}}$. As described in [9],

an approximate model can be used for surfaces with amphoteric groups. The amphoteric groups can be modeled as a combination of negatively and positively ionizable surface groups. A group can be either neutral or charged (negatively or positively depending on the group type). The different groups are treated independently, and the total number of binding sites for both group types is equal to the total number of amphoteric sites.

Using the relationships $K_A = [H_S^+]\Gamma^{O-}/\,\Gamma^{\mathrm{OH}}$ and $K_B = [H_S^+]\Gamma^{\mathrm{OH}}/\,\Gamma^{\mathrm{OH}_2^+}$, 2 pK model surface charge can be expressed as

$$\sigma_0 = \frac{-e\Gamma}{1+\frac{\left[H_S^+\right]}{K_A}} + \frac{e\Gamma}{1+\frac{K_B}{\left[H_S^+\right]}}. \tag{9}$$

The proton activity between the solid surface $[H_S^+]$ and the bulk $[H_B^+]$ is described by the Boltzmann relation at the thermal equilibrium as

$$\left[H_S^+\right] = \left[H_B^+\right]\exp\left(-\frac{e(\Psi_0 - V_{\mathrm{REF}})}{kT}\right). \tag{10}$$

Introducing (10) to (9) leads to

$$\sigma_0 = \frac{-e\Gamma}{1+\left(\frac{\left[H_B^+\right]}{K_A}\right)\exp\left(\frac{-e(\Psi_0-V_{\mathrm{REF}})}{kT}\right)} + \frac{e\Gamma}{1+\left(\frac{K_B}{\left[H_B^+\right]}\right)\exp\left(\frac{e(\Psi_0-V_{\mathrm{REF}})}{kT}\right)}. \tag{11}$$

The expression for Ψ_0 can be obtained from (3)–(5) as $\Psi_0 = (\sigma_0 + C_{\mathrm{SG}}V_{\mathrm{FG}} + C_{\mathrm{Stern}}\Psi_{\mathrm{DL}})/(C_{\mathrm{SG}} + C_{\mathrm{Stern}})$. There is a constant potential drop between the RE and the electrolyte solution [27]. We set this constant to zero in the simulations and consider V_{REF} equal to the solution bulk potential.

The oxide surface charge in the (11) depends on both V_{FG} and pH_B of the solution. This shows that these parameters together set the surface charge and both of these parameters can be used to charge or discharge the surface and to control the ionic screening layer.

To solve the entire electrochemical system, another independent expression between σ_0 and Ψ_{DL} is required. This can be obtained from the Grahame equation

$$\sigma_{\mathrm{DL}} = \frac{2\epsilon_w\epsilon_0 kT}{e\lambda_D}\sinh\left(\frac{e(\Psi_{\mathrm{DL}} - V_{\mathrm{REF}})}{2kT}\right) \tag{12}$$

from which the independent expression is given as

$$\sigma_0 = C\frac{2\epsilon_w\epsilon_0 kT}{e\lambda_D}\sinh\left(\frac{e(\Psi_{\mathrm{DL}} - V_{\mathrm{REF}})}{2kT}\right) + C_{\mathrm{SG}}(\Psi_{\mathrm{DL}} - V_{\mathrm{FG}}) \tag{13}$$

where $C = (C_{\mathrm{SG}} + C_{\mathrm{Stern}})/C_{\mathrm{Stern}}$ and λ_D is the Debye screening length [28]. The system can be solved by taking the intersection of the two σ_0 and Ψ_{DL} curves.

IV. Results and Discussion

A. Sensitivity of the ISFGFET

Our transistor structure has two inputs: 1) the CG and 2) the SG. Both input nodes can be used to change the output of the device. We define two device sensitivities: 1) the CG sensitivity and 2) the SG sensitivity. Sensitivity is the change in the output (I_D) per unit change in the measurand at the input (either V_{CG} or Ψ_0). There is a fundamental tradeoff between the sensitivities. To understand this, we differentiate (2), which yields

$$\Delta V_{\mathrm{FG}} = \frac{C_{\mathrm{CG}}}{C_{\mathrm{TOT}}}\Delta V_{\mathrm{CG}} + \frac{C_{\mathrm{SG}}}{C_{\mathrm{TOT}}}\Delta\Psi_0. \tag{14}$$

The above reveals that the ISFGFET is inherently less sensitive than ISFET. In an ISFET, the oxide above the transistor channel is directly in contact with the electrolyte solution, and thus, it can sense the full voltage shift in the sensing surface. In the ISFGFET, the sensitivity of the second term is weighted with the ratio of the SG capacitance and the total capacitance of the system. This SG coupling coefficient is always between zero and one and thus weakens the sensitivity of the sensor. To have the ability to control the device operating point while maintaining considerable sensitivity, these capacitances should be in the same order of magnitude.

B. Programming of the Surface

We used the presented model to predict the behavior of the ISFGFET with various surface and electrolyte solution parameters. We investigated the impact of both pH_B and V_{FG} on Ψ_0. In all computations, the RE was grounded, and the ionic strength was $c_0 = 10$ mM. An SG oxide thickness of 10 nm and the resulting oxide field strength $E_{\mathrm{SG}} = (V_{\mathrm{FG}} - \Psi_0)/d$ was used in the simulations. We use the electric field rather than V_{FG} to present the results, since it is the electric field strength over the sensing oxide that determines the stimulus for surface programming rather than the absolute value of V_{FG}. In addition, it allows comparison between different oxide thicknesses. V_{FG} can be controlled through the CG, but first we consider the relationship between the FG and the electrolyte solution. When pH_B was swept in the simulations [Fig. 2(a) and (c)], V_{FG} was set to zero potential.

In Fig. 2(a), the dependence of the surface potential Ψ_0 on pH_B is shown. An inert surface with no ionizable groups shows no pH_B sensitivity. With a large number of surface sites, the surface response approaches that of a Nernstian surface with the theoretical limit of $\Delta\Psi_0 \approx 59$ mV/pH_B. Between the extremes are the non-Nernstian surfaces that exhibit interesting behavior. Near the point-of-zero-charge (PZC), the sensitivity decreases as expected. However, much clearer sensitivity reduction happens when the surface saturates. In a saturated surface, there are no longer surface sites available for ionization and the surface then behaves as it was inert. This is a direct result of the surfaces buffering capacity, or the lack of it.

In Fig. 2(b), a surface with high density of ionizable groups N_S exhibits high buffering. When V_{FG} is swept, Ψ_0 remains unchanged due to the buffering of the surface [9]. Buffering is the ability of the surface to counter the changing electric field by protonating or deprotonating. When the electric field is exerted normal to the surface, it causes the ionizable groups at the surface to respond. This response counters the change in the surface charging from V_{FG}.

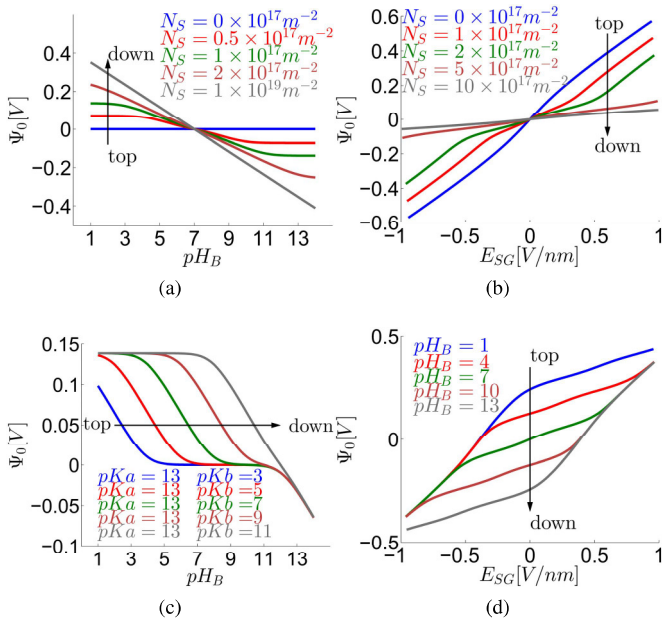

Fig. 2. Relationship of surface potential Ψ_0 to pH_B and E_{SG} with varying ionizable site density and dissociation constants. The parameters used in the simulations unless otherwise stated were $\mathrm{pK}_A = 8$, $\mathrm{pK}_B = 6$, $\mathrm{pH}_B = 7$, $c_0 = 10$ mM, $\epsilon_r = 9.3$, $d = 10$ nm, and $V_{\mathrm{REF}} = 0$. In (b) and (d), V_{FG} was swept from -10 to 10 V resulting in the shown SG field strength $E_{\mathrm{SG}} = (V_{\mathrm{FG}} - \Psi_0)/d$. (a) Surface pH_B sensitivity with different ionizable group densities. (b) Relation between E_{SG} and Ψ_0 with different ionizable group densities. (c) Effect of surface dissociation constant separation with $N_S = 1 \times 10^{17}$ m^{-2}. (d) Effect of pH_B on E_{SG} to Ψ_0 relationship with $Ns = 2 \times 10^{17}$ m^{-2}.

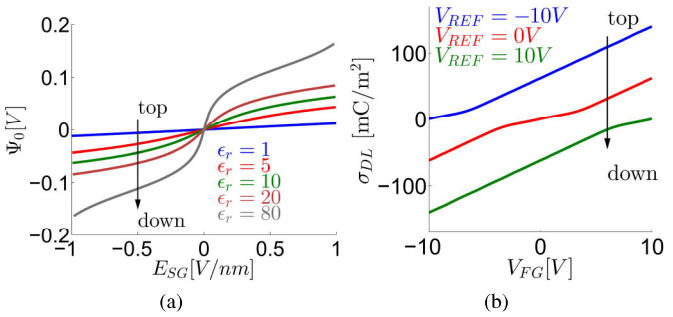

Fig. 3. (a) Coupling strength increase (via increasing oxide ϵ_r) between the electrolyte solution and the surface. The used simulation parameters were $N_S = 5 \times 10^{18}$ m^{-2}, $\mathrm{pK}_A = 9$ and $\mathrm{pK}_B = 5$, $\mathrm{pH}_B = 7$, $V_{\mathrm{REF}} = 0$ and $c_0 = 10$ mM. (b) Diffuse layer charge simulated with V_{REF} values of -10, 0, and 10 V, with $N_S = 1 \times 10^{18}$ m^{-2}, $\mathrm{pK}_A = 8$, $\mathrm{pK}_B = 6$, and $\epsilon_r = 9.3$. In all three cases, the double layer charging is determined by the potential across the electrolyte solution.

With high N_S, only a small fraction of ionizable sites is required to compensate ΔV_{FG} and Ψ_0 varies only little and shows a linear response. If, however, N_S is lowered, the effect of changing V_{FG} becomes more apparent. A surface with N_S equal to 0.1 or 0.2 in units of nm^{-2} shows a region near zero-field strength with a gently sloping region. As the field strength increases as a result of increased V_{FG}, the slope abruptly steepens and runs in parallel with an inert surface with no ionizable groups. Then, all ionizable groups have shifted from a neutral state to an ionized state and the surface can no longer function as a buffer. An inert surface clearly shows the potential change in the surface. However, due to the small capacitance C_{SG} compared with that of the double layer, the V_{FG} coupling is weak and there is only a modest change in Ψ_0 in all cases compared with the change in V_{FG}. The apparent nonlinearity in the potential in the inert case is due to the nonlinearity of the double layer capacitance.

In Fig. 2(c), the effect of dissociation constant separation on Ψ_0 is simulated. pK_A is kept constant, but pK_B is changed from 3 to 11. The similarity and the sigmoidal shape of the curves are apparent. The change in the dissociation constant merely shifts the region where the surface is pH_B sensitive. The width of the flat part increases with increasing pK separation. When the two pK values are sufficiently close to each other, no apparent gap is seen. However, closer examination reveals that the sensitivity is reduced from ~35 to 29 mV/pH around the PZC. It is also clear that when the pK_B value is increased and the surface is reacting with higher pH values (lower $[H_S^+]$), the pH insensitive regions at low pH values are wider. The PZC of the surface is found at the midpoint of the pK values as $\mathrm{pH}_{PZC} = (\mathrm{pK}_A + \mathrm{pK}_B)/2$.

In Fig. 2(d), Ψ_0 is examined with several pH_B values with varying insulator field strength. The flat part in the curves presents the buffering region. Lowering pH_B (increase in $[H_S^+]$) positively charges the surface. This also shifts the buffering region to positive FG potentials. Then, increasing the potential at the FG will repel the native positive charging at the surface. With a negative V_{FG}, the positive charge further accumulates to the surface. Since the surface has a positive native charge, the buffering limit is reached with the modest negative voltages with a low pH_B compared with a high pH_B.

C. Dielectric Breakdown

A fundamental limit of electrofluidic gating with ISFGFET arises from the dielectric breakdown limit. Reported breakdown electric field values for common oxides Al_2O_3, SiO_2, and Si_3N_4 are 0.62, 0.56, and 0.24 V/nm, respectively [29].

The effect of the insulator dielectric constant ϵ_r, and thus the insulators coupling strength is investigated in Fig. 3(a). Common insulators have a dielectric constant in the range of 4–5, but high-k dielectrics can have much higher dielectric constants. In the simulation, five dielectric constants in the range of 1–80 are examined. The increase in coupling amplifies the impact of electrofluidic gating and higher potentials can be achieved at the sensing surface as well as at the diffusion layer. This also allows the usage of thicker dielectrics while maintaining the same capacitance values and the engineering of the electric field strengths to a level that does not exceed the maximum field strengths of the oxides. However, the high local fields in high-k dielectrics make them more susceptible for breakdown. It has been found that such a material breakdown roughly follows $k^{-1/2}$ dependence [30]. This dependence still does not exclude their use in strengthening the coupling between V_{FG} and Ψ_0. Fig. 3(b) shows that an increase in ϵ_r increases the impact of the coupling of the potential more than the corresponding

reduction in the maximum dielectric field strength in a high-k material.

Another electric field limitation arises from the C_{CG} field strength. The FG and its potential can be controlled via the CG. Thus, it is the gate used to control the charging of the sensing surface. As we indicated in Section IV-A, the change in V_{CG} is multiplied a $C_{\mathrm{CG}}/C_{\mathrm{TOT}} < 1$ to yield the corresponding change in V_{FG}. Thus, to change the potential at FG, the CG potential must increase in potential multiplied with the inverse of this capacitance ratio. Thus, the SG sensitivity must be allowed to reduce to have realizable field strengths in C_{CG}. This is an inherent SG sensitivity and electrofluidic gating tradeoff.

The electrofluidic gating seems plausible in semiconductor devices. However, for practical purposes, the material dielectric strength, dielectric constant, and thickness of the oxides need to be specified to a suitable compromise depending on the application.

D. Transistor Operation Point and Screening Layer Tuning

Both Ψ_0 and Ψ_{DL} closely track V_{REF} changes when V_{FG} is not controlled. This can be explained through the much larger capacitances describing the double layer compared with the relatively small capacitances of the electronic part. σ_{DL} is defined through the Grahame equation (12) and it depends on the potential difference over the diffusion layer. The potentials Ψ_0 and Ψ_{DL} change in respect to the ground, whereas the potential differences $(V_{\mathrm{REF}} - \Psi_{\mathrm{DL}})$ and $(V_{\mathrm{REF}} - \Psi_0)$ remain static on V_{REF} changes. If this potential difference over the diffusion layer does not change, then neither does σ_{DL}.

The electrofluidic gating, however, requires control over σ_{DL}. This is obtained through the simultaneous control of V_{FG} and V_{REF} that determines the potential across the sensing branch (the stack from the FG to the RE). The result is shown in Fig. 3(b) where σ_{DL} is plotted against V_{FG} with different V_{REF} values. This shows that both the RE and the FG can be used to control the ionic screening layer charge. Thus, we can simultaneously optimize the transistor operating point and the charging of the fluidic part of the sensor. This indicates that the electrofluidic gating can be enhanced through the use of RE and not only rely on V_{CG} induced changes in V_{FG} for electrofluidic gating. In addition, the pH can used for chemical biasing [9] of the surface to shift the surface charge to a desired level. With the added control of biasing the surface, there is more freedom in engineering the capacitance field strengths and device sensitivities to practical levels while maintaining the property of electrofluidic gating.

E. Operation Modes

1) ISFGFET-Mode: V_{FG} depends on both V_{CG} and Ψ_0. The charges at the CG are abundant and the potential is independent on Ψ_0. On the other hand, the nonlinear Ψ_0 is determined by the electrolyte solution condition as well as V_{FG}. The change in the ISFGFET operation is best described by the change in the threshold voltage. The ISFGFET threshold seen from the CG is

$$V_{\mathrm{CG}}^{T} = \frac{C_{\mathrm{TOT}}}{C_{\mathrm{CG}}} V_{\mathrm{FG}}^{T} - \frac{C_{\mathrm{SG}}}{C_{\mathrm{CG}}} \Psi_0\left(V_{\mathrm{FG}}^{T}, \Psi_0\right) - \frac{Q}{C_{\mathrm{CG}}} \qquad (15)$$

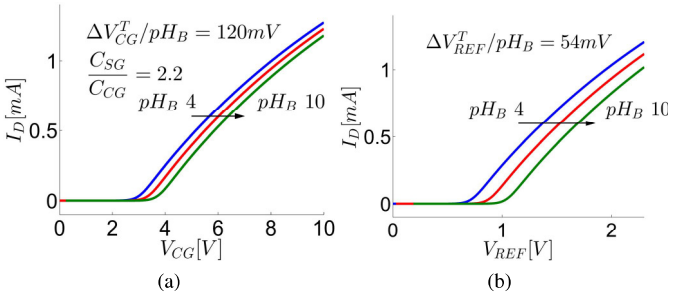

Fig. 4. (a) ISFGFET threshold shift. The response to pH_B is modeled as Al_2O_3 surface with $c_0 = 10$ mM, $V_D = 0.1$ V and $V_{\mathrm{REF}} = 0$ V. (b) ISFET threshold shift. V_{REF} is swept. The simulation considers CG as uncoupled. Note the difference in x-axis scales.

where V_{FG}^{T} is the FG threshold voltage and other parameters are as defined in Section II.

In Fig. 4(a), we simulate the sensor V_{CG} versus I_D curves with several pH_B values with a grounded RE and zero net charge. We simulate the sensing surface as an Al_2O_3 with a thickness of 6 nm. Fig. 4(a) shows that an increase in pH_B (decrease in $[H_B^+]$) shifts V_{CG}^{T} to the right due to the negative surface charging. An increase in pH_B ideally decreases the surface potential approximately 59 mV/pH_B and to overcome the reduction of Ψ_0 at the FG, V_{CG} must be increased. $\Delta V_{\mathrm{CG}}/\mathrm{pH}_B$ shown in Fig. 4(a) is clearly higher than the Nernstian limit. This does not mean that the ISFGFET is super-Nernstian. It is actually a result of weaker coupling between the CG and the FG compared SG with FG. Thus, V_{CG} must increase more than the corresponding potential decrease in the sensing surface.

Our intention in the simulations is to elucidate the difference of the ISFGFET and ISFET modes and the effect of capacitance ratios in the sensor structure. However, it should be noted that the surfaces with a high number of ionizable surface groups (Nernstian surfaces), such as Al_2O_3, have high buffering capacity and therefore the amount of surface charge modulation is minimal in the simulated example. According to the simulations, a non-Nernstian surface in a suitable pH range and with the interplay with V_{CG} and RE potential, the useful conditions for electrofluidic gating can be obtained.

2) ISFET-Mode: The ISFGFET can be operated similarly as an ISFET. If the CG capacitance is small compared with C_{SG}, the coupling between the CG and the FG is weak. As a result, the device no longer responds to V_{CG}. In such a case, the construction resembles the conventional ISFET with an added series capacitor. Then, the sensitivity of the device is at its maximum but the ability to probe the ionic screening layer is lost. The ISFET-mode simulation result is shown in Fig. 4(b).

V. Experimental Verification

A. Device

The ISFGFET utilizes an enhancement mode nMOS. The SG and the FG are connected through aluminum wire. The SG has an Si_3N_4 passivation layer. The layer was cut using reactive-ion etching exposing the underlaying aluminum sensing probe. Aluminum forms a native oxide in air. We use this as the pH sensing layer. The estimated the thickness of this

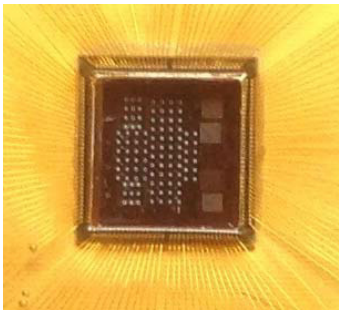

Fig. 5. Photograph of the SU-8 encapsulated chip.

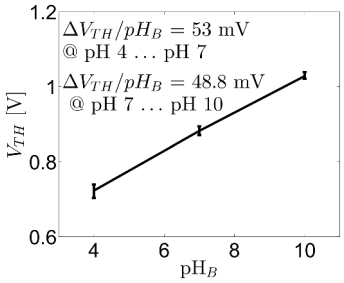

Fig. 6. ISFGFET pH_B sensitivity characterization in the pH_B values of 4, 7, and 10.

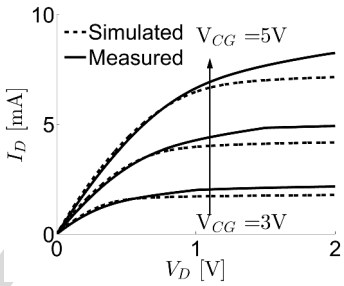

Fig. 7. Transistor transfer characteristics. I_D versus V_D, with V_{CG} values of 3–5 V. $V_{FG} \approx 1/2 \times V_{CG}$.

layer is 6 nm. We concluded from energy-dispersive X-ray spectroscopy measurement that a typical native oxide thickness was formed [31]. The sensing area was 20×24 μm^2.

In Fig. 5, we show the photograph of the SU-8 encapsulated chip from the top showing the SU-8 formed well and the bonding wires at the edge of the chip. The chip was mounted on a printed circuit board (PCB) through the pins on its backside. The PCB provides routing of signals from the chip to the measurement equipment. More detailed description of the device has been given earlier [20].

We used SU-8 negative-tone photoresist to encapsulate the bonded wires and to form a well on the transistor area of the chip. Due to the high viscosity of SU-8, the substrate was heated prior to applying the SU-8 on it. This reduces viscosity and ensures smoother flow with minimal stress on the wirebonds. The chip was then prebaked for 9 h at 95 °C. The temperature ramp-up and ramp-down was done with the modest temperature change to ensure low heat stress. Then, the chip was soaked in 50 mL of SU-8 developer overnight with moderate stir using a magnetic stir bar. Finally, the SU-8 encapsulation was rinsed with isopropanol and then with DI water.

B. Electrical Characterizations

The electrical characterizations of the device were conducted with an Agilent 4142B parameter analyzer. In pH sensing measurements, 20 μL of pH 4, 7, and 10 buffer solutions (Oakton) were introduced, respectively, in the SU-8 well on the chip. The source, drain, and substrate electrodes of a single transistor on the chip were connected through the PCB to the Agilent analyzer. An external Ag/AgCl RE was immersed into the solution and connected to the analyzer to provide bias to the sensor.

C. pH Sensitivity

We investigated the pH sensitivity of ISFGFET in standard pH buffers of value 4, 7, and 10 in the ISFET mode. Fig. 6 collects the results from five consecutive set of measurements. The average threshold variation is 53.0 mV/pH from pH 4 to pH 7 and 48.8 mV/pH from pH 7 to pH 10. The threshold increases from pH 4 to pH 10. This is due to decreasing Ψ_0 which for nMOS-type device leads to decreased current. Thus, the change in threshold voltage is equal to the change in the surface potential, but of opposite polarity. As our simulations suggest, the high number of ionizable groups in Al_2O_3 leads to near Nernstian pH response, and thus high buffering capacity of the surface and consequently to minimal ability for electrofluidic gating. In order to achieve proper capability of electrofluidic gating, the number of the ionizable groups must be reduced.

D. Transistor Transfer Characteristics

The presented model incorporates a SPICE model (electrical part) and an oxide/electrolyte solution interface model. The SPICE model simulates the nMOS part of the device, i.e., the relationship between V_{FG} and I_D. This is merged to the electrochemical system and to the capacitive network via MATLAB.

First, we checked the validity of the SPICE model. In Fig. 7, the transistor is measured in its pristine state in dry conditions without any charging at the SG. The potential is applied through the CG and the SG is floating. The SPICE model predicts well the measured behavior, but in saturation region, the measured current is on average $\sim$1.2 times larger. Although the bias in this case is applied through the CG, we expect the small mismatch to be a result of the V_{FG} and I_D relationship mismatch. We use this correction factor throughout the subsequent measurement results to correct the SPICE model by multiplying the model I_D with it.

We investigated the transistor threshold voltage seen from the CG to validate the SPICE models threshold voltage predictions. We measured I_D while sweeping V_{CG}. From the measurement, the threshold voltage was extracted. The sensor with the passivation layer cut had a threshold value as expected and no correction to it was required.

E. ISFET Transfer Characteristics

The chemical system considered here comprises two surface interfaces, the oxide/solution interface and the

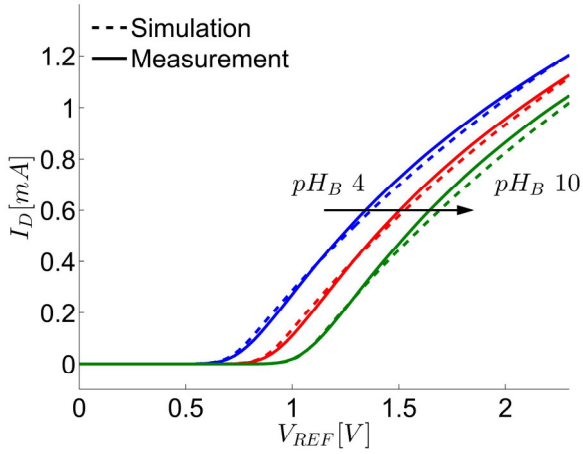

Fig. 8. ISFET-mode transfer characteristics and pH sensitivity comparison between model and experiments in the pH_B values of 4, 7, and 10. V_D is 0.1 V.

RE/solution interface. In earlier simulations, we assumed no potential drop at the latter interface for convenience. In reality, there is a constant potential drop associated to it. It is ideally constant, but generally unknown. In our model, we can estimate from the drain current V_{FG} and subsequently Ψ_0. V_{REF} is also known. Therefore, the only unknown is the potential drop between the RE and the solution bulk potential. We computed the RE potential drop from the measured threshold voltages in three pH measurements (pH 4, pH 7, and pH 10). The average potential drop from the three measurements when compared with the model revealed that the solution bulk potential is 71 mV lower than the applied V_{REF}. We apply this potential drop to the simulation throughout when we compare the model to experiments.

It has to be noted that the RE potential drop directly affects the threshold voltage and it is indistinguishable from the other threshold voltage shifting mechanisms. Since the measured pristine state threshold voltage of the transistor agrees with the simulated V_{TH} seen from the CG, we attribute the measured difference purely to the RE potential drop. Any other factor deviating the threshold voltages cannot be identified, since the computed potential drop is only known through the model/experiment comparison. For example, a constant offset in Ψ_0 would lead to a constant threshold shift. However, the oxide pH sensitivity and pH_{PZC} is well known from the previous studies and therefore we expect the computed RE potential drop to present quite accurately its true value.

In Fig. 8, we compare the simulation to experiments in three buffer solutions with the pH_B values of 4, 7, and 10. V_{REF} is swept from 0 to 2.5 V, and the constant drain voltage is 0.1 V. The model agrees well with the simulation in terms shape of the curves, their pH sensitivity and in the absolute value of V_{REF} and I_D. The transconductance reduction of the device is investigated by comparing the MOSFET model that excludes the CG and the SG to the ISFET-mode transfer characteristics. In addition, the transconductance reduction is almost negligible due to the large C_{SG}.

VI. Conclusion

We have shown an ISFET variant that utilizes an FG structure with two input nodes, the CG and the RE. A weighted sum of these input voltages along with the net charge at the FG determines V_{FG}. In comparison with ISFET, the ISFGFET has an added CG that allows simultaneous control over the transistor bias point and the ionic screening layer. The cost of having the ability to optimize both the transistor bias point and the sensors fluidic part is the reduced sensing surface sensitivity compared with an ISFET that couples the surface potential (Ψ_0) directly to the FET channel through a gate oxide. Moreover, it was shown that the surface functionalization has profound effects on the fluidic field-effect response. High ionizable surface site density results in high pH sensitivity and mitigates the possibility to tune the surface and screening layer. Oxides commonly have a hydroxyl group density of 4–12/nm^{-2} [26]. Such a high density of ionizable sites leads to only a small fraction of these groups being ionized in realizable oxide field strengths. The fluidic field effect can be enhanced by a decrease in the surface pH sensitivity accompanied with increased coupling between V_{FG} and Ψ_0. We discussed how both the transistor operation point and the ionic screening layer charge can be tuned to a desired level. We envision that this ability to optimize the electronic part of the ISFGFET as well as the fluidic part can serve to improve, e.g., the sensitivity when the sensor is used to measure biological recognition events. The model was verified thorough the ISFET mode where agreement between the pH_B sensitivity, transfer characteristics and in threshold voltage as well as in I_D in absolute terms were found.

Acknowledgment

The authors would like to thank Prof. I. Kymissis's Research Group for their valuable contribution and the chip encapsulation.

References

[1] P. Bergveld, "Development of an ion-sensitive solid-state device for neurophysiological measurements," *IEEE Trans. Biomed. Eng.*, vol. BME-17, no. 1, pp. 70–71, Jan. 1970.

[2] J. M. Rothberg *et al.*, "An integrated semiconductor device enabling non-optical genome sequencing," *Nature*, vol. 475, pp. 348–352, Jul. 2011.

[3] N. Y.-M. Shen, Z. Liu, C. Lee, B. A. Minch, and E. C.-C. Kan, "Charge-based chemical sensors: A neuromorphic approach with chemoreceptive neuron MOS (CνMOS) transistors," *IEEE Trans. Electron Devices*, vol. 50, no. 10, pp. 2171–2178, Oct. 2003.

[4] K. Levon, A. Rahman, T. Sai, and B. Zhao, "Floating gate field effect transistors for chemical and/or biological sensing," U.S. Patent 7 462 512 B2, Dec. 9, 2008.

[5] K. Levon, A. Rahman, T. Sai, and B. Zhao, "Floating gate field effect transistors for chemical and/or biological sensing," U.S. Patent 7 884 398 B2, Feb. 8, 2011.

[6] M. Barbaro, A. Bonfiglio, and L. Raffo, "A charge-modulated FET for detection of biomolecular processes: Conception, modeling, and simulation," *IEEE Trans. Electron Devices*, vol. 53, no. 1, pp. 158–166, Jan. 2006.

[7] P. Georgiou and C. Toumazou, "CMOS-based programmable gate ISFET," *Electron. Lett.*, vol. 44, no. 22, pp. 1289–1290, Oct. 2008.

[8] K. Jayant *et al.*, "Programmable ion-sensitive transistor interfaces. I. Electrochemical gating," *Phys. Rev. E*, vol. 88, p. 012801, Jul. 2013.

[9] Z. Jiang and D. Stein, "Electrofluidic gating of a chemically reactive surface," *Langmuir*, vol. 26, no. 11, pp. 8161–8173, 2010.

[10] R. E. G. van Hal, J. C. T. Eijkel, and P. Bergveld, "A novel description of ISFET sensitivity with the buffer capacity and double-layer capacitance as key parameters," *Sens. Actuators B, Chem.*, vol. 24, nos. 1–3, pp. 201–205, 1995.
[11] S. Martinoia, G. Massobrio, and L. Lorenzelli, "Modeling ISFET microsensor and ISFET-based microsystems: A review," *Sens. Actuators B, Chem.*, vol. 105, no. 1, pp. 14–27, 2005.
[12] K. Ghowsi and R. J. Gale, "Field effect electroosmosis," *J. Chromatogr. A*, vol. 559, nos. 1–2, pp. 95–101, 1991.
[13] R. B. M. Schasfoort, S. Schlautmann, J. Hendrikse, and A. van den Berg, "Field-effect flow control for microfabricated fluidic networks," *Science*, vol. 286, no. 5441, pp. 942–945, 1999.
[14] D. Stein, M. Kruithof, and C. Dekker, "Surface-charge-governed ion transport in nanofluidic channels," *Phys. Rev. Lett.*, vol. 93, p. 035901, Jul. 2004.
[15] R. Karnik, K. Castelino, and A. Majumdar, "Field-effect control of protein transport in a nanofluidic transistor circuit," *Appl. Phys. Lett.*, vol. 88, no. 12, p. 123114, 2006.
[16] F. Fixe, H. M. Branz, N. Louro, V. Chu, D. M. F. Prazeres, and J. P. Conde, "Immobilization and hybridization by single sub-millisecond electric field pulses, for pixel-addressed DNA microarrays," *Biosensors Bioelectron.*, vol. 19, no. 12, pp. 1591–1597, 2004.
[17] K. Jayant *et al.*, "Programmable ion-sensitive transistor interfaces. II. Biomolecular sensing and manipulation," *Phys. Rev. E*, vol. 88, p. 012802, Jul. 2013.
[18] W. Guan, N. K. Rajan, X. Duan, and M. A. Reed, "Quantitative probing of surface charges at dielectric–electrolyte interfaces," *Lab Chip*, vol. 13, no. 7, pp. 1431–1436, 2013.
[19] Y. Liu, P. Georgiou, T. Prodromakis, T. G. Constandinou, and C. Toumazou, "An extended CMOS ISFET model incorporating the physical design geometry and the effects on performance and offset variation," *IEEE Trans. Electron Devices*, vol. 58, no. 12, pp. 4414–4422, Dec. 2011.
[20] Q. Zhang *et al.*, "Surface functionalization of ion-sensitive floating-gate field-effect transistors with organic electronics," *IEEE Trans. Electron Devices*, vol. 62, no. 4, pp. 1291–1298, Apr. 2015.
[21] T. Shibata and T. Ohmi, "A functional MOS transistor featuring gate-level weighted sum and threshold operations," *IEEE Trans. Electron Devices*, vol. 39, no. 6, pp. 1444–1455, Jun. 1992.
[22] Y. Hu and P. Georgiou, "A robust ISFET pH-measuring front-end for chemical reaction monitoring," *IEEE Trans. Biomed. Circuits Syst.*, vol. 8, no. 2, pp. 177–185, Apr. 2014.
[23] S. Meyburg, "Transistor arrays for the direct interfacing with electrogenic cells," Ph.D. dissertation, RWTH Aachen Univ., Aachen, Germany, 2005.
[24] R. E. G. van Hal, J. C. T. Eijkel, and P. Bergveld, "A general model to describe the electrostatic potential at electrolyte oxide interfaces," *Adv. Colloid Interf. Sci.*, vol. 69, nos. 1–3, pp. 31–62, 1996.
[25] S. Martinoia and G. Massobrio, "A behavioral macromodel of the ISFET in SPICE," *Sens. Actuators B, Chem.*, vol. 62, no. 3, pp. 182–189, 2000.
[26] M. Kosmulski, "Oxide/electrolyte interface: Electric double layer in mixed solvent systems," *Colloids Surf. A, Physicochem. Eng. Aspects*, vol. 95, nos. 2–3, pp. 81–100, 1995.
[27] P. Bergveld, "ISFET, theory and practice," in *Proc. IEEE Sensor Conf.*, Toronto, ON, Canada, Oct. 2003.
[28] J. N. Israelachvili, *Intermolecular and Surface Forces*. Waltham, MA, USA: Academic, 2011.
[29] H. Bartzsch *et al.*, "Electrical insulation properties of sputter-deposited SiO_2, Si_3N_4 and Al_2O_3 films at room temperature and 400 °C," *Phys. Status Solidi A*, vol. 206, no. 3, pp. 514–519, 2009.
[30] J. W. McPherson, J. Kim, A. Shanware, H. Mogul, and J. Rodriguez, "Trends in the ultimate breakdown strength of high dielectric-constant materials," *IEEE Trans. Electron Devices*, vol. 50, no. 8, pp. 1771–1778, Aug. 2003.
[31] K. Wefers and C. Misra, "Oxides and hydroxides of aluminum," Alcoa Lab., New York City, NY, USA, Tech. Rep. 19, 1987, p. 64.

Matti Kaisti received the B.Sc. degree in electrical engineering from the Turku University of Applied Sciences, Turku, Finland, in 2008, and the M.Sc. degree in electrical engineering from the University of Turku, Turku, in 2012, where he is currently pursuing the Ph.D. degree in electronics with a concentration on biosensing applications.

He was an RF Design Engineer with DA-Design OY, Jokioinen, Finland, from 2008 to 2012, developing radars and radiometers.

Qi Zhang received the B.Eng. degree in materials science and engineering from Donghua University, Shanghai, China, in 2008, and the Ph.D. degree in materials chemistry from New York University (NYU), Brooklyn, NY, USA, in 2014.

He is currently a Post-Doctoral Research Fellow at NYU, collaborating with several New York-based biotech start-ups to develop electrochemical biosensing devices for medical diagnostics.

Alok Prabhu received the master's and Ph.D. degrees in biomedical engineering from the Polytechnic Institute, New York University (NYU), Brooklyn, NY, USA, in 2007 and 2012, respectively.

He was a Post-Doctoral Researcher at NYU, where he was involved in the design and development of electrochemical assays for the ion-sensitive floating gate field effect transistor biosensor platform.

Ari Lehmusvuori received the M.Sc. and Ph.D. degrees in molecular biotechnology and diagnostics from the University of Turku, Turku, Finland, in 2008 and 2014, respectively.

He has focused on rapid DNA diagnostics and fluorescence reporter technology development, and recently expanded his focus also on the label-free field-effect transistor based DNA sensing.

Arifur Rahman (SM'–) received the B.S. degree in electrical engineering from the Polytechnic Institute, New York University, Brooklyn, NY, USA, the M.S. and Ph.D. degrees in electrical engineering from the Massachusetts Institute of Technology, Cambridge, MA, USA, and the M.B.A. degree from Santa Clara University, Santa Clara, CA, USA.

He is currently a Program Director and an Architect with Altera Corporation, San Jose, CA, USA.

Kalle Levon received the B.Sc. and M.Sc. degrees from the University of Helsinki, Helsinki, Finland, and the Ph.D. degree from The University of Tokyo, Tokyo, Japan.

He joined the Polytechnic Institute, New York University, Brooklyn, NY, USA, in 1989, as a Professor, where he is the Chairman and Vice Provost of research. His current research interests include nonequilibrium phase separations and organic electronics.